

RESEARCH ARTICLE

10.1029/2018JD029601

A New 200-Year Spatial Reconstruction of West Antarctic Surface Mass Balance

Yetang Wang¹ , Baojuan Huai¹, Elizabeth R. Thomas² , Michiel R. van den Broeke³ , J. Melchior van Wessem³, and Elisabeth Schlosser^{4,5} 

Key Points:

- A new reconstruction of spatially complete surface mass balance over the West Antarctic Ice Sheet during the past 200 years is presented
- West Antarctica experiences a significant negative SMB trend during the nineteenth century, but a significant positive trend during 1900–2010
- The WAIS east-west dipole SMB trends are associated with positive polarity of Southern Annular Mode (SAM) and dominant La Niña events

Supporting Information:

- Supporting Information S1

Correspondence to:

Y. Wang,
wangyetang@163.com

Citation:

Wang, Y., Huai, B., Thomas, E. R., van den Broeke, M. R., van Wessem, J. M., & Schlosser, E. (2019). A new 200-year spatial reconstruction of West Antarctic surface mass balance. *Journal of Geophysical Research: Atmospheres*, 124. <https://doi.org/10.1029/2018JD029601>

Received 1 SEP 2018

Accepted 13 APR 2019

Accepted article online 23 APR 2019

¹College of Geography and Environment, Shandong Normal University, Jinan, China, ²British Antarctic Survey, Cambridge, UK, ³Institute for Marine and Atmospheric Research Utrecht (IMAU), Utrecht University, Utrecht, The Netherlands, ⁴Department of Atmospheric and Cryospheric Sciences, University of Innsbruck, Innsbruck, Austria, ⁵Austrian Polar Research Institute, Vienna, Austria

Abstract High-spatial resolution surface mass balance (SMB) over the West Antarctic Ice Sheet (WAIS) spanning 1800–2010 is reconstructed by means of ice core records combined with the outputs of the European Centre for Medium-Range Weather Forecasts “Interim” reanalysis (ERA-Interim) and the latest polar version of the Regional Atmospheric Climate Model (RACMO2.3p2). The reconstruction reveals a significant negative trend (-1.9 ± 2.2 Gt/year-per decade) in the SMB over the entire WAIS during the nineteenth century, but a statistically significant positive trend of 5.4 ± 2.9 Gt/year-per decade between 1900 and 2010, in contrast to insignificant WAIS SMB changes during the twentieth century reported earlier. At regional scales, the Antarctic Peninsula and western WAIS show opposite SMB trends, with different signs in the nineteenth and twentieth centuries. The annual resolution reconstruction allows us to examine the relationships between SMB and large-scale atmospheric oscillations. Although SMB over the Antarctic Peninsula and western WAIS correlates significantly with the Southern Annular Mode due to the influence of the Amundsen Sea Low, and El Niño/Southern Oscillation during 1800–2010, the significant correlations are temporally unstable, associated with the phase of Southern Annular Mode, El Niño/Southern Oscillation and the Pacific decadal oscillation. In addition, the two climate modes seem to contribute little to variability in SMB over the whole WAIS on decadal-centennial time scales. This new reconstruction also serves to identify unreliable precipitation trends in ERA-Interim and thus has potential for assessing the skill of other reanalyses or climate models to capture precipitation trends and variability.

1. Introduction

Mass loss from the West Antarctic Ice Sheet (WAIS) contributes significantly to current global mean sea level rise, and in the future may potentially raise global mean sea level by about 3.3 m if disintegrated entirely (Bamber et al., 2009). Its mass budget is balanced between ice dynamical loss driven by basal melting and calving of icebergs, and the net result of precipitation, surface sublimation, drifting-snow driven erosion/deposition and sublimation, and surface meltwater runoff, the sum of which comprises the surface mass balance (SMB). Various methods have revealed that the WAIS has been experiencing mass loss at an accelerating rate in recent decades, which points to a dynamic imbalance primarily attributable to a sustained increase in ice wastage from the Amundsen Sea embayment and the western Antarctic Peninsula (AP; e.g., Mouginit et al., 2014; Rignot, 2008; Shepherd et al., 2018; Wouters et al., 2015). Conversely, knowledge of long-term variability of WAIS SMB is greatly insufficient due to the sparseness of instrumental data, associated with the remoteness of the ice sheet. In addition, the existing snow accumulation measurements typically sample one dimension at the cost of the others. For example, stake farms can reproduce spatial variability at the local scale but are limited to short time spans. Ice cores provide long-term records but suffer from limited spatial coverage. These deficiencies become key constraints for the estimate of WAIS mass imbalance and its response to recent climate changes.

Compared with in situ measurements, climate models or reanalysis products are more complete in both time and space and offer important resources for continental scale SMB assessments. Global reanalysis products are created by assimilating meteorological observations into numerical weather prediction models. Among various global reanalysis products, the European Centre for Medium-range Weather Forecasts “Interim” reanalysis (ERA-Interim) is most likely to reasonably reproduce Antarctic snow accumulation variability

since 1979 (Bromwich et al., 2011; Wang et al., 2016). However, large biases still exist because some processes influencing SMB such as refreezing, diamond dust (clear-sky precipitation), and drifting snow are not parametrized in ERA-Interim. Regional climate models can be coupled with a multilayer snow model, a firn densification model, snow albedo and drifting snow schemes, etc. They are forced by global atmospheric reanalyses at the lateral and upper boundaries and have proven to realistically simulate Antarctic SMB and its components (e.g., Lenaerts et al., 2012; Van Wessem et al., 2014, 2018). Regional climate models represent spatial patterns of SMB better than the reanalyses, but potentially perform poorer in capturing interannual variability (e.g., Medley et al., 2013; Wang et al., 2015, 2016), because no observations are assimilated into the models. This has been partly resolved by applying upper air relaxation (Van de Berg & Medley, 2016). Global climate models predict that WAIS SMB will increase in response to climate warming during the remainder of the 21st century (e.g., Agosta et al., 2013; Frieler et al., 2015), largely because of the increase in atmospheric water vapor following the Clausius-Clapeyron relation. Nevertheless, ice core records in the vicinity of the WAIS ice divide reveal a variable relationship between SMB and air temperature during the past 31,000 years (Fudge et al., 2016).

Given the respective advantages and disadvantages of in situ measurements and climate model simulations, statistical methods have been used to reconstruct Antarctic SMB by combining the sparse field observations and climate models or reanalyses accordingly (Monaghan et al., 2006; Rotschky et al., 2007; Van de Berg et al., 2006). However, these reconstructions are based either on multiyear averaged in situ observations or ice core records from the mid-1950s onward, and do not examine spatial patterns of SMB variability on multidecadal to centennial time scales. Longer-term and spatiotemporally more complete SMB data sets are still required to characterize SMB variability on these longer time periods, so as to determine whether recent SMB changes are part of a longer-term trend potentially related to anthropogenic climate forcing. These data sets are also useful for estimating mass balance variability.

Thomas et al. (2017) compiled all available ice core snow accumulation rates over Antarctica and assessed regional SMB variability on centennial scales. Based on the compilation by Thomas et al. (2017), Wang et al. (2017) revealed regional differences of SMB variability over the WAIS from 1900 to 2010, and their robust relationships with a deepening of the Amundsen Sea Low (ASL) and regional sea ice anomalies in the ASL region. However, the large distances between ice core sites bring substantial challenges in estimating SMB over the whole WAIS. In addition, sea ice anomalies and the ASL deepening are sensitive to large-scale climate variability modes such as Southern Annular Mode (SAM) and El Niño–Southern Oscillation (ENSO; e.g., Raphael et al., 2016; Turner et al., 2013), and thus, WAIS SMB should be associated with the two climate modes. Yet the relationship between WAIS SMB and the two climate modes has not been fully understood.

Here, we present a new high-spatial resolution WAIS SMB reconstruction that aims to better understand its spatial and temporal variability during the past two centuries, and its relationship with the SAM and ENSO. This new reconstruction combines ice core snow accumulation records and outputs of global reanalysis products and regional climate models, using a proven kriging-like interpolation method to generate a continuous trend surface, which can better represent spatial patterns of SMB than a regional average of the ice core records as done by Thomas et al. (2017) and Wang et al. (2017).

2. Data and Methods

2.1. Data

To reconstruct the gridded SMB fields for the WAIS, we use the precipitation and sublimation fields from ERA-Interim (Dee et al., 2011), which best represent interannual variability in observed Antarctic snow accumulation among the available reanalyses (Bromwich et al., 2011; Wang et al., 2016). We also use outputs of the latest polar version of the Regional Atmospheric Climate Model (RACMO2.3p2; Van Wessem et al., 2018). This version upgrades the previous versions by including upper-air relaxation, tuned parameters in the cloud scheme, and improved calculation of surface albedo. ERA-Interim and RACMO2.3p2 are bilinearly interpolated to a common 25×25 km² polar stereographic grid.

The available snow accumulation observations consist of 38 ice core records with annual resolution from the PAGES (Past Global Changes) Antarctic 2k database (Thomas et al., 2017), which have been quality-

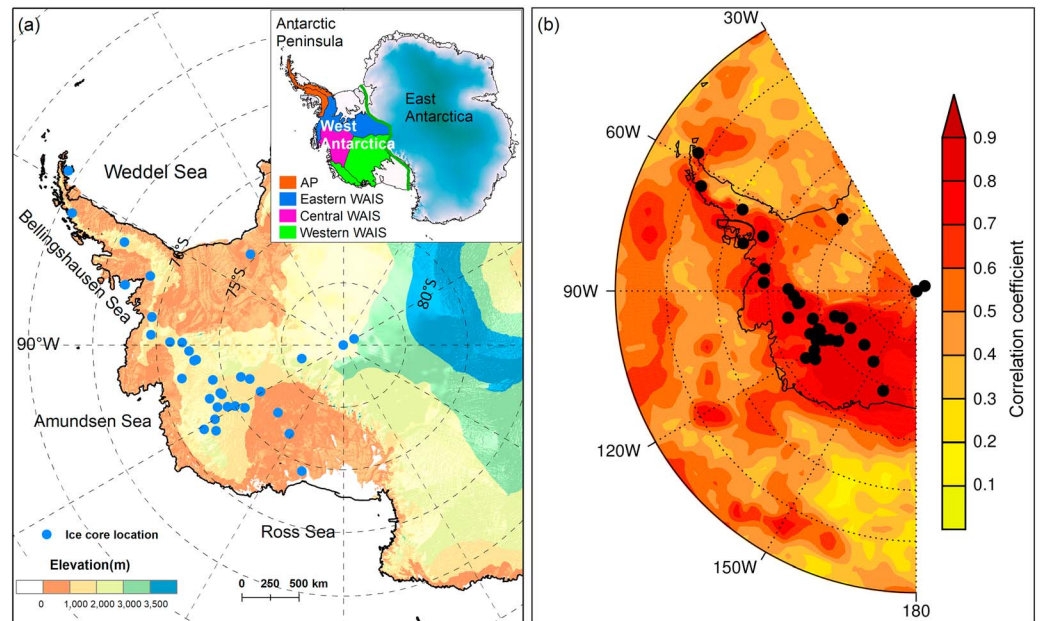


Figure 1. (a) The locations of ice core drilling sites on the WAIS. The inset shows the boundaries of the four subregions. (b) Composite map of the maximum absolute Pearson's correlation coefficients between each of ice core records at 36 sites (black dots) and ERA-Interim $P - E$ fields over the WAIS (i.e., this map is a composite of 36 maps). WAIS = West Antarctic Ice Sheet.

controlled and corrected for layer thinning due to snow densification and ice flow. These records, of which 31 span more than 100 years, 18 more than 200 years and three ~2,000 years, are well distributed over the WAIS (Figure 1a). Detailed information for each ice core record is provided in Table S1. For the reconstruction, two ice core records covering <20 years were omitted, and in six cores, data gaps were filled using the method described in detail in the supporting information. The number of cores for the reconstruction by year from 1800 to 2010, and the locations of the cores available for four full time slices (1800–1850, 1850–1900, 1900–1950, and 1950–2010) are shown in Figure 2. Postdepositional processes affect the spatial representativeness of the individual ice cores; nevertheless, the composite map of the maximum correlation at each grid cell between individual ice cores and the corresponding ERA-Interim annual precipitation minus evaporation ($P - E$) anomaly with respect to the 1980–1989 mean (the reference period) reveals significant correlations ($r > 0.5$, $p < 0.01$) over most of the WAIS (Figure 1b). This supports our assumption that spatially coherent accumulation patterns represented by the available ice core records cover almost the whole WAIS and that the impact of noise from local perturbations is minor for our reconstruction; it will therefore be neglected in this study.

2.2. Methods

2.2.1. Reconstruction

First, we calculate the relative difference of annual SMB with respect to the reference period for each ice core. Similarly, ERA-Interim anomalies of annual $P - E$ are calculated relative to the 10-year mean reference. Then, a gridded product of annual SMB anomalies spanning 1800–2010 for the WAIS is created using the kriging-like technique developed by Monaghan et al. (2006). We further improved this using kriging weights following Nicolas and Bromwich (2014) to avoid overfitting the model. The main equation of the interpolation algorithm is

$$\Delta Y(s, t) = \sum_{k=1}^N \eta_k(s) w_k(s) \Delta u_k(t) \quad (1)$$

where $\Delta Y(s, t)$ is the SMB anomaly predicted at a given time (t) and a given location or grid point s , as a combination of the SMB anomaly Δu_k , $k=1, 2, \dots, N$ ice cores used in the interpolation; $\eta_k(s)$ is 1 or -1 dependent on the sign of the correlation between the k th core and location s . The $w_k(s)$ stands for the weight (w) assigned to the k th core at the location s and is calculated by

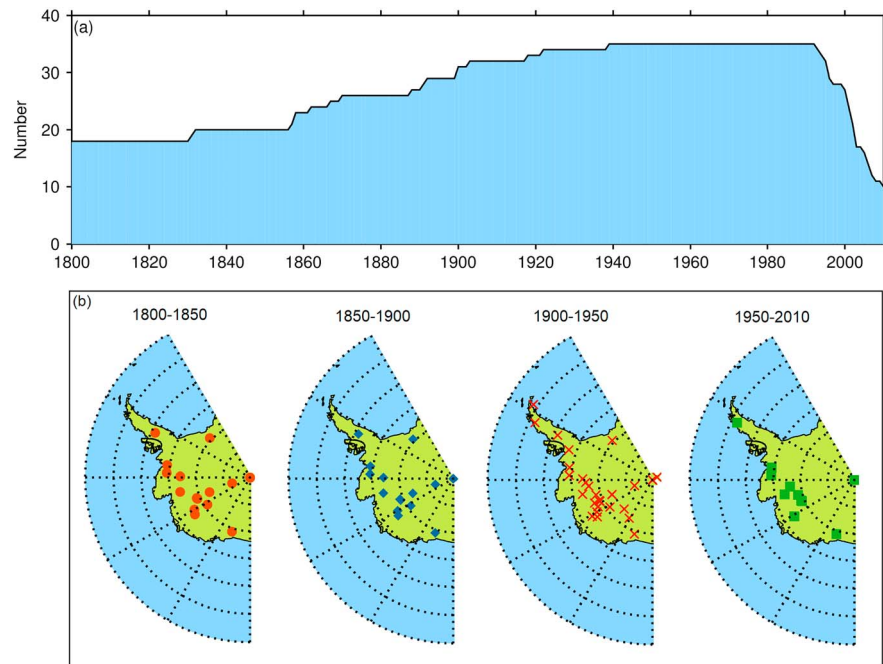


Figure 2. (a) Numbers of ice cores for surface mass balance reconstruction during 1800–2010. (b) The locations of the cores available for four full time slices (1800–1850, 1850–1900, 1900–1950, and 1950–2010).

$$w_k(s) = \frac{r_k(s)^2}{\sum_{k=1}^N r_k(s)^2} \quad (2)$$

where $r_k(s)$ is the Pearson's correlation coefficient between $P - E$ at the location s of the k th core SMB records and the time series of $P - E$ fields. The correlation coefficients are calculated for the period 1979–2010 based on the linearly detrended ERA-Interim data. Finally, since RACMO2.3p2 represents multiyear averaged SMB better than ERA-Interim (Wang et al., 2016), we convert the annual snow accumulation anomalies into SMB records using the 1980–1989 mean SMB from RACMO2.3p2 to replace that from ERA-Interim at each grid point. Before the conversion, RACMO2.3p2 SMB fields are further calibrated by accounting for the bias between the ice core records and the simulated mean SMB for their overlapping period (1980–1989; details can be found in the supporting information).

Despite all efforts made to fill data gaps, a few ice core records are still incomplete for the 1800–2010 period. Here, we make full use of the large overlapping regions between some ice cores' spatial footprints of correlations for the reconstruction. A different set of weights are calculated by removing the ice cores with missing data to reconstruct SMB over the years for which data gaps appear.

2.2.2. Validation of Reconstruction

The robustness of the SMB reconstruction is estimated using a split sample calibration-verification test method, which has been used for estimating reconstruction of Antarctic temperature (Nicolas & Bromwich, 2014) and pressure (Fogt et al., 2018). The full period (1979–2010) is split into two nonoverlapping 16-year periods (1979–1994 and 1995–2010). When one subperiod is used to determine the kriging weights and to produce a SMB reconstruction, another subperiod yields an independent validation of the reconstruction. The final estimate is the mean of the two sets of statistics. The Pearson's coefficient of correlation (r), reduction of error (RE) and coefficient of efficiency (CE) are used as the validation statistics. The mathematical definitions of RE and CE are presented in the supporting information. To decrease the influence of spurious trends in ERA-Interim, the linearly detrended time series are used to calculate r , RE, and CE.

2.2.3. Uncertainty Calculation

Uncertainty in our reconstruction includes measurement errors, that is, small-scale perturbations in the ice core records largely caused by postdepositional processes, errors of spatial kriging interpolation, and

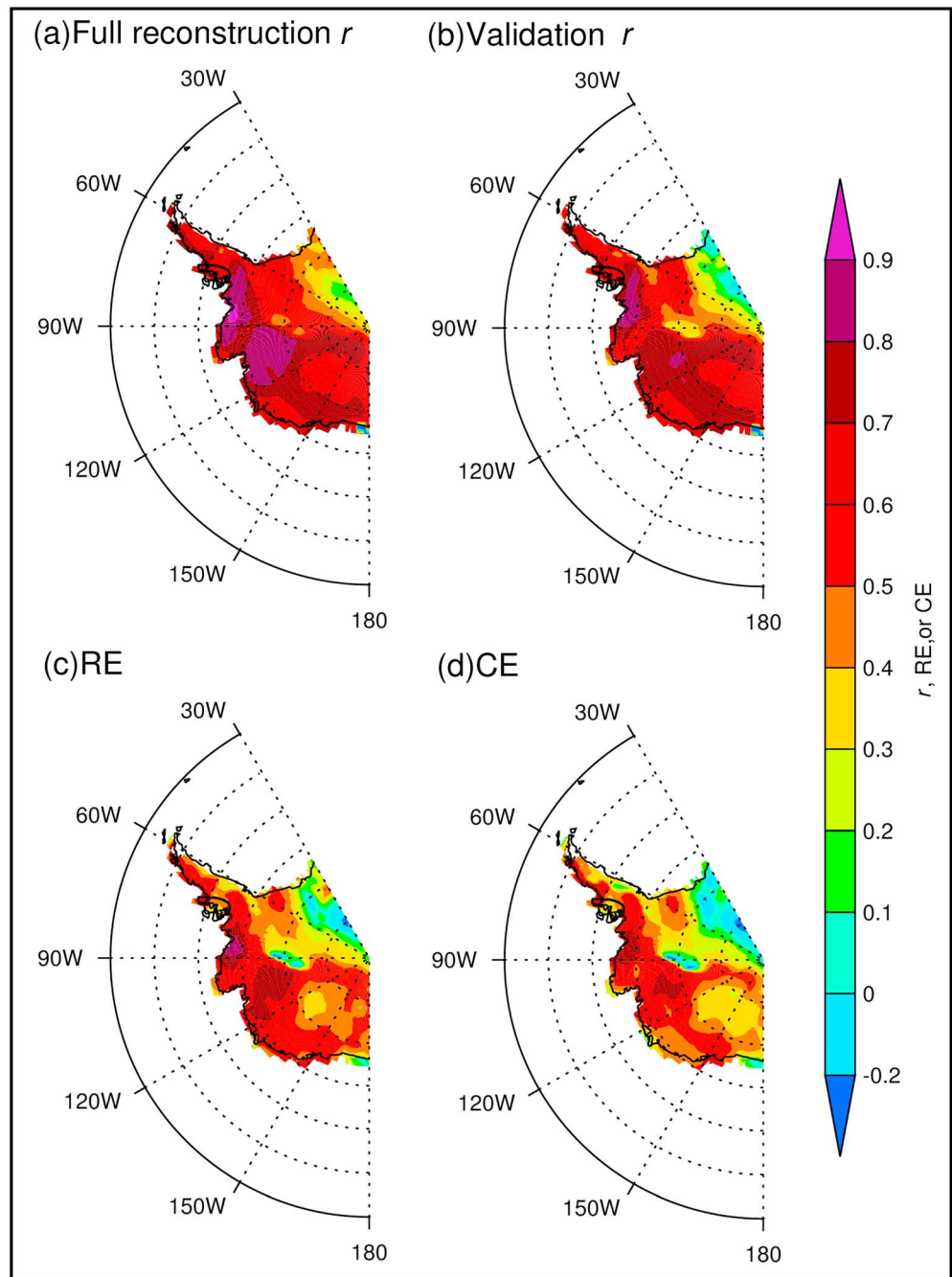


Figure 3. Skill statistics for surface mass balance reconstruction relative to ERA-Interim, 1979–2010. (a) Full reconstruction correlation, (b) verification reconstruction correlation, (c) RE, and (d) CE. RE = reduction of error; CE = coefficient of efficiency.

uncertainty in ERA-Interim and RACMO2.3p2. We calculate the root-mean-square error (RMSE) between the detrended record and ERA-Interim $P - E$ time series at the location of each ice core, and the standard deviation of the reanalysis time series. As suggested by Medley and Thomas (2019), the minimum of the standard deviation and RMSE is approximated as the observational uncertainty in each ice core and then propagated year-by-year and grid-by-grid. The uncertainty in the spatial kriging technique can be estimated by the RMSE between the original ERA-Interim snow accumulation data and the reconstructed $P - E$ records based on this method using ERA-Interim $P - E$ times series at each ice core site (Medley & Thomas, 2019). While ERA-Interim can well represent the interannual variability in snow accumulation

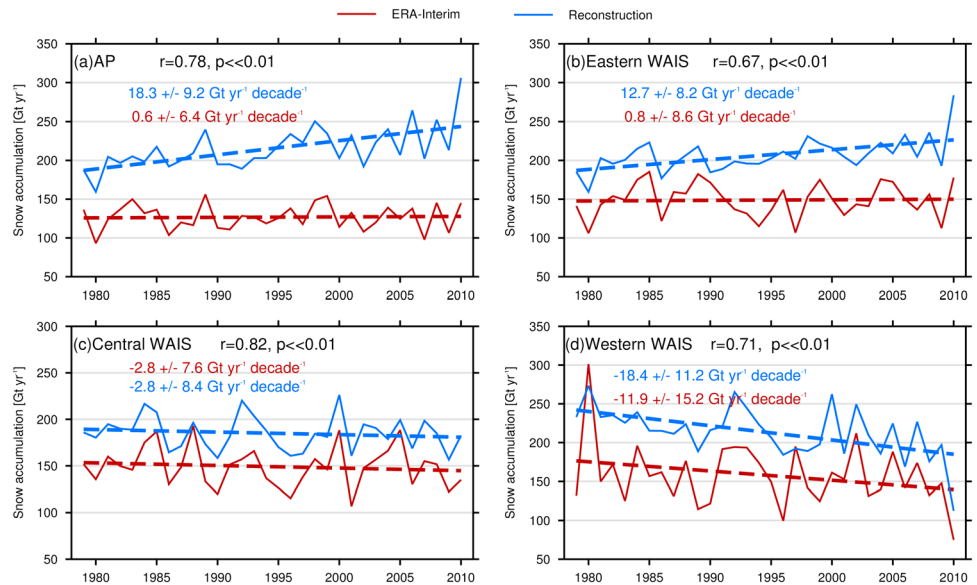


Figure 4. (a) Reconstructed surface mass balance and ERA-Interim $P - E$ averaged over the (a) AP, (b) eastern WAIS, (c) central WAIS, and (d) western WAIS for the 1979–2010 period. Correlation coefficient (r) is calculated by detrended time series. The uncertainty of trends for reconstruction is $2\sigma_r$, and for ERA-Interim is doubled standard error of the regression coefficient. AP = Antarctic Peninsula; WAIS = West Antarctic Ice Sheet.

observations (Wang et al., 2016), some unreliable trends in this reanalysis are still present, which affects the determination of kriging weighting. To reduce this, we use the detrended time series when calculating correlation coefficients between ice core record and reanalysis $P - E$ fields. Because biases in the averaged SMB over the 1980–1989 period in RACMO2.3p2 are corrected as described above, the uncertainty in this model is not considered in the estimate of final uncertainty. A final evaluation of our reconstruction uncertainty is generated by the square root of the sum of the squared measurement and spatial kriging interpolation errors.

When calculating snow accumulation trend uncertainty, reconstruction errors are also considered by means of a Monte Carlo method. We perform $n = 10,000$ Monte Carlo simulations of snow accumulation time series for each grid point by adding random noise with a normal distribution of a mean of zero and variance equal to the squared reconstruction uncertainty. We then recalculate the trends of the n simulation series at each grid and lead to a variance (σ_m) of the distribution of these trends. The final trend uncertainty (σ_r) is the square root of the sum of σ_m and squares of standard error of the regression coefficients. We apply $\pm 2\sigma_r$ for trend uncertainty throughout this study.

3. Results and Discussion

3.1. Evaluation of Reconstruction Skill

The skill of our reconstruction is assessed with respect to ERA-Interim $P - E$. Our comparison of time series is made using the relative reconstructions to avoid bias from the large spread in mean annual snow accumulation. Figure 3 demonstrates the statistics of the reconstruction skill at each WAIS grid point. For both the full and validation reconstructions, the correlation coefficient values are typically greater than 0.6 ($p < 0.01$) at most grid cells of the WAIS, suggesting the general agreement between the reconstruction and ERA-Interim. Consistent with correlations, the resulting RE and CE are higher than zero across the overwhelming majority of the WAIS, supporting the validity of our reconstruction. Low correlations only occur on parts of the Filchner Ice Shelf and the interior of the eastern WAIS, which may be related to the lack of ice cores in these regions. On the very few grid points of these regions, negative CE values are also present, which reveals that the reconstructions are inferior to those using the climatological mean. Nevertheless, we cannot rule out the possibility that the errors occur in ERA-Interim in some regions, but not in our reconstruction.

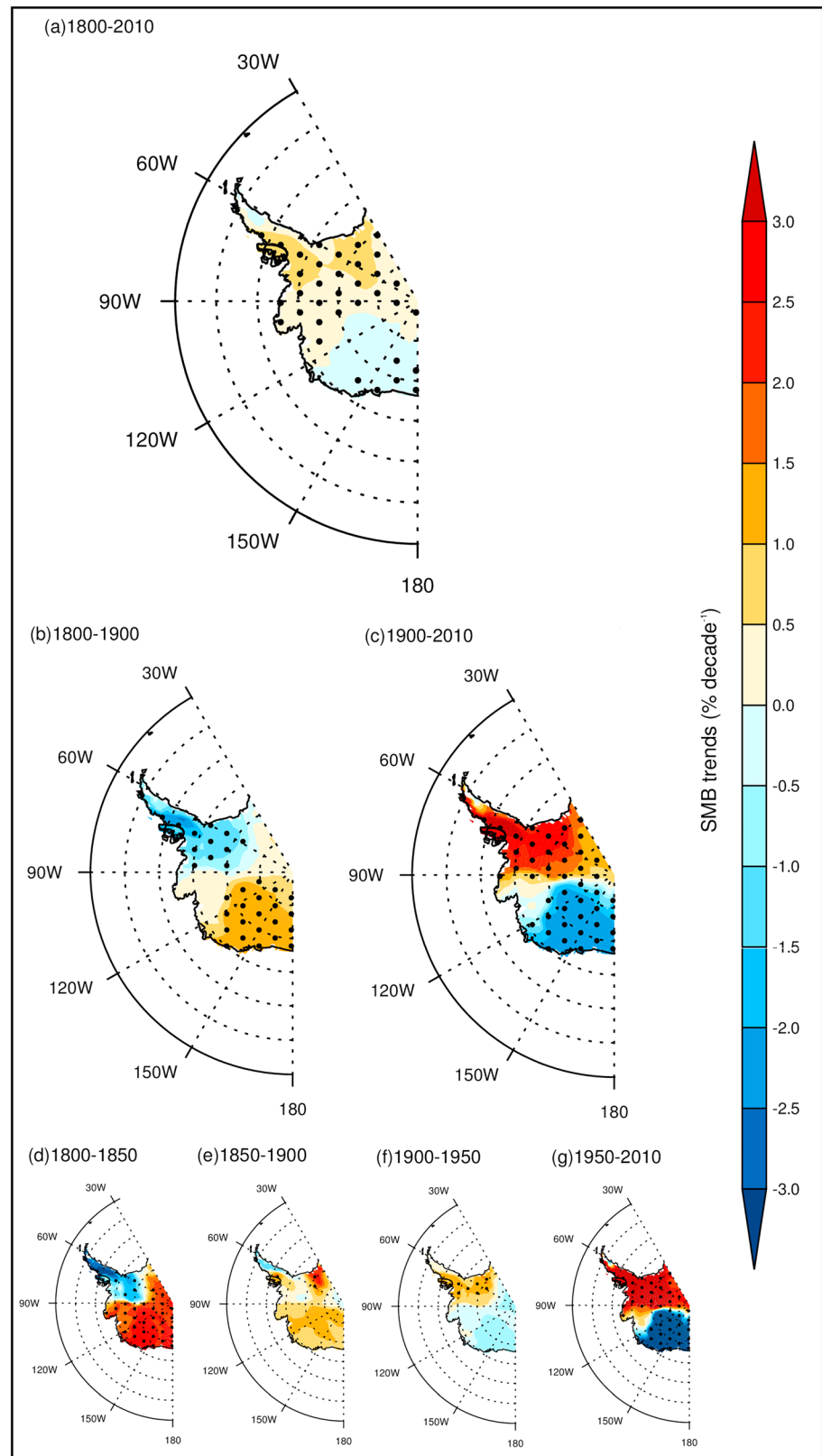


Figure 5. Spatial distribution of linear trends in reconstructed SMB anomalies relative to the mean 1980–1989, for the (a) 1800–2010, (b) 1800–1900, (c) 1900–2010, (d) 1800–1850, (e) 1850–1900, (f) 1900–1950, and (g) 1950–2010 periods. Dotted regions indicate confidence is reached at the 99% level. SMB = surface mass balance.

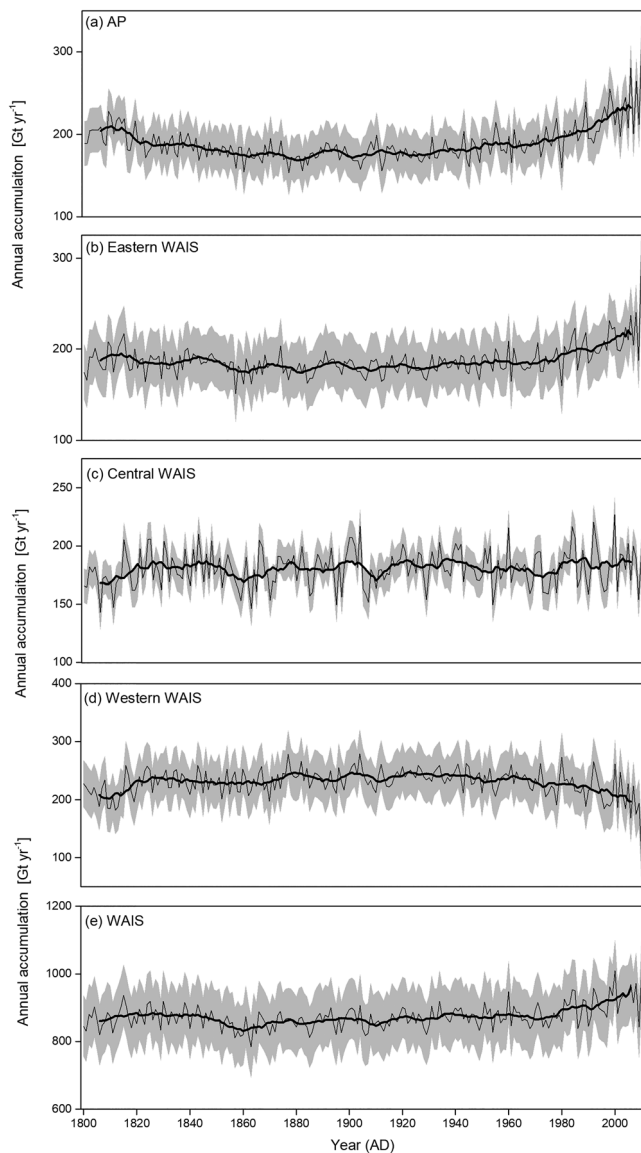


Figure 6. Time series of reconstructed annual mean SMB from 1800 to 2010, spatially averaged over the (a) AP, and (b) eastern, (c) central, and (d) western WAIS. The gray shading indicates the uncertainty interval ($\pm 1\sigma$) of our reconstruction (see section 2.2.3 uncertainty calculation). SMB = surface mass balance; WAIS = West Antarctic Ice Sheet.

Our SMB reconstruction shows significant correlations with the original ERA-Interim $P - E$ averaged over the AP, and eastern, central, and western WAIS, with $r > 0.65$ ($p < 0.01$). However, large differences in temporal trend between the reconstruction and simulation occur over the AP and eastern WAIS as can be seen in Figure 4. This is attributed to spurious ERA-Interim $P - E$ trends over the two regions because our reconstruction only uses spatial patterns from ERA-Interim and temporal patterns from ice core records. The more reliable trends in the reconstruction than ERA-Interim are further confirmed by the comparison of trends in ice core SMB records and ERA-Interim for their overlapping period (Table S2). Another possible reason is the relatively low performance of the reconstruction for the interior of the eastern WAIS associated with lack of ice cores.

To examine if our reconstruction is greatly affected by one or more ice core records, 36 reconstructions where each ice core record is excluded one-by-one, are performed by using the remaining ice core records. We compare the difference between the independent excluded location reconstructed SMB and the full reconstruction at the excluded locations from the subsamples in the jackknifing method. The small difference ($< 2\%$) at any year of the past two centuries suggest that our reconstruction is insensitive to the removal of the data (Figure S2). This is further confirmed by the regression slope (0.95 ± 0.08) between SMB trends for the independent location reconstruction and the full reconstruction at the excluded locations for the 1800–2010 period.

3.2. Comparison With Other Spatial SMB Reconstructions

Monaghan et al. (2006) created a kriging-like interpolation method and reconstructed gridded Antarctic SMB from 1955 to 2004 based on ice core records and ERA-40 precipitation fields. In this reconstruction, no significant SMB trends are found since 1955. However, our reconstruction reveals a significant positive trend (11.8 ± 7.2 Gt/year per decade) during the same period. This difference may result from more recent ice core records in the AP and coastal areas used for our reconstruction than the Monaghan et al. (2006) reconstruction. The latter is heavily weighted by the ice cores from inland Antarctica. Most recently, Medley and Thomas (2019) generated a spatial SMB reconstruction over the AIS between 1801 and 2000, using the kriging-like interpolation method created by Monaghan et al. (2006), based on 53 ice core records and three atmospheric reanalysis products. The kriging-like method accounts for every observation contribution, no matter whether some of the observations are collinear. This increases the risk of overfitting in the reconstruction by Medley and Thomas (2019), especially for the WAIS with the clustering

of observations. In our reconstruction, the improvements by Nicolas and Bromwich (2014) are utilized to optimize the weighting coefficients to avoid overfitting the model by taking into account the relationships between ice core records. We also use linearly detrended reanalysis time series (not performed in the Medley & Thomas, 2019, reconstruction) to calculate the weighting coefficients, which help to minimize the impact of suspicious trends in ERA-Interim $P - E$ fields. In addition, the kriging-like method improved by Nicolas and Bromwich (2014) also ensures the best match between the reconstructed values and the observations. SMB time series from our reconstruction spatially averaged over the AP, and eastern, central, and western WAIS are compared with those from the reconstruction by Medley and Thomas (2019; Figure S3). There are high and significant correlations between our reconstruction and the Medley and Thomas (2019) reconstruction for each region average, with r values greater than 0.9 ($p \ll 0.01$), which is somewhat expected due to their common method basis.

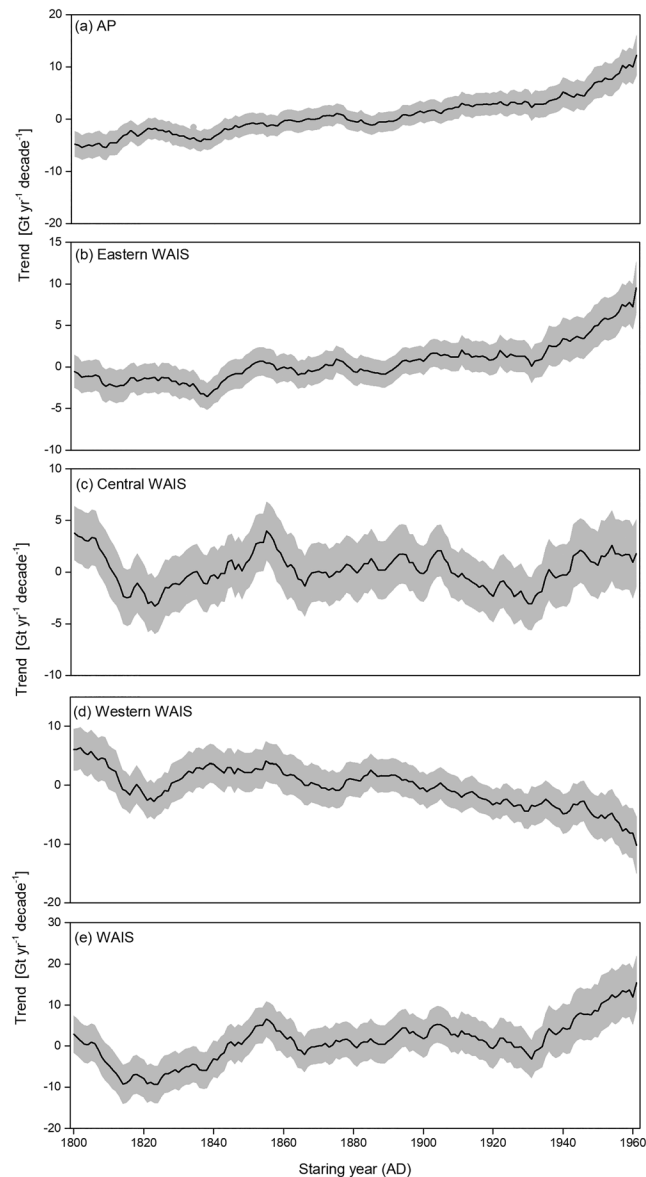


Figure 7. The 30-year running trends for reconstructed SMB time series, spatially averaged over the (a) AP, (b) eastern, (c) central, (d) western, and (e) whole WAIS. The gray shading represents $2\sigma_t$ uncertainties. SMB = surface mass balance; WAIS = West Antarctic Ice Sheet; AP = Antarctic Peninsula.

3.3. SMB Variability During the Past 200 Years

Based on this new reconstructed SMB data set, a history of WAIS SMB variability during the 19th, 20th, and early 21st century is presented. We first investigate the spatial patterns of WAIS SMB variability trends for the 1800–2010 period, and 50- and 100-year time intervals starting in 1800 CE (Figure 5). Over 1800–2010, statistically significant but opposing trends exist between the western (negative trend) and eastern (positive trend) WAIS. This dipole pattern prevails in the 100-year time slices, but with a change in sign between the nineteenth and twentieth centuries. The western WAIS SMB trend is significantly positive for 1800–1900, but negative for 1900–2010, while the opposite occurs in the eastern WAIS and at the AP. Furthermore, the dipole shaped trend patterns are larger and more significant for the 1800–1850 (Figure 5d) and 1950–2010 (Figure 5g) periods. On the other hand, there are almost no significant trends during 1850–1900 and 1900–1950.

Based on the regional differences in Figure 5, we calculate the time series of annual and 11-year smoothed SMB (Figures 6a–6d) averaged over the AP, and eastern, central, and western WAIS (boundary lines can be found in the Figure 1a inset). In the nineteenth century, SMB averaged over the AP exhibits a significantly negative trend (-3.0 ± 1.3 Gt/year per decade) while a significantly positive trend (2.4 ± 1.7 Gt/year per decade) is found over the western WAIS. Opposite trends between AP and western WAIS are found for the 1900–2010 period, with significant magnitudes of 5.0 ± 1.5 and -4.1 ± 1.9 Gt/year per decade, respectively. Over the eastern WAIS, there is no noticeable change before 1960, but since then SMB significantly increased by 8.8 ± 3.6 Gt/year per decade. In the last 200 years, the trends are insignificant for the central WAIS. For the entire nineteenth century, a statistically significant negative trend (-1.9 ± 2.2 Gt/year per decade) occurs over the whole WAIS. However, a statistically significant increase is found over the whole WAIS for the 1900–2010 period (5.4 ± 2.9 Gt/year per decade), and for the 1950–2010 period, which is different from previous studies, which show insignificant changes in WAIS snow accumulation since 1955 (Monaghan et al., 2006) and during the past 200 years (Frezzotti et al., 2013). This may result from the lack of recent ice core records in these studies, especially in the AP and coastal areas, and the assignment of high weight to inland Antarctic sites.

SMB trends calculated for the 50-year running windows over the WAIS, and its four subregions are illustrated in Figure 7. The gray shading shows the trend uncertainties ($\pm 2\sigma_t$). Since around 1940, the AP and eastern WAIS display large and statistically significant positive trends in SMB ($p < 0.01$), whereas trends for the western WAIS are significantly negative.

In particular, for SMB over the AP and eastern WAIS, the most recent 50-year (1961–2010) trend exceeds any earlier 50-year trends, as demonstrated in Thomas et al. (2017). In contrast, SMB trend for the western WAIS during the same period exhibits the most negative value during the past 200 years, and it is significant at $p < 0.01$. The trends observed in the most recent 50-year periods for the central WAIS fall within the range of all 50-year trends since 1800. After about 1950, the 50-year trends for the WAIS time series are significantly positive.

3.4. Relationship Between SMB Variability and SAM and ENSO

Changes in snow accumulation over the WAIS are linked to both SAM (e.g., Goodwin et al., 2016; Thomas et al., 2008) and ENSO (e.g., Ding et al., 2011; Genthon & Cosme, 2003; Kaspari et al., 2004; Marshall et al., 2017). The SAM is the leading mode of atmospheric circulation variability in the high latitudes of the Southern Hemisphere, reflecting the atmospheric pressure gradient between middle and high latitudes.

Table 1

Correlation Coefficient (r) and Corresponding Significance (p) Between SMB Over the West Antarctic Ice Sheet (WAIS) and Its Four Subregions, and SOI for the 1866–2010 period, the Marshall (2003) SAM Index (SAMM, 1957–2010), SAM Indices Reconstructed by Fogt (2009; SAMF, 1905–2004), Abram et al. (2014; SAMA, 1800–2005), and Dätwyler et al. (2017; SAMD, 1800–2005), Respectively

Index	AP	Eastern WAIS	Central WAIS	Western WAIS	WAIS
SAMM (1957–2010)	0.61	0.52	0.06	-0.49	0.06
SAMF (1905–2004)	0.39	0.33	0.01	-0.28	0.07
SAMD (1800–2005)	0.53	0.44	0.11	-0.25	0.09
SAMA (1800–2005)	0.43	0.36	-0.04	-0.35	-0.02
SOI (1866–2010)	0.27	0.25	-0.1	-0.31	-0.14

Note: Bold font indicates that the correlations are at the 99% confidence level. SOI = Southern Oscillation Index; SMB = surface mass balance; SAM = Southern Annular Mode.

The ENSO teleconnection is through a Rossby wave train of geopotential height anomalies originating in the tropical Pacific during ENSO events, known as the Pacific South American (PSA) pattern (e.g., Mo & Higgins, 1998; Schneider et al., 2012). The PSA pattern is defined as second empirical orthogonal functions of extratropical geopotential height fields (SAM is the leading empirical orthogonal function; Mo & Higgins, 1998). To examine the relationship between the reconstructed WAIS SMB and the SAM and ENSO, we use the observation-based SAM index by Marshall (2003) for the 1957–2010 period, termed as SAMM, and the SAM indices reconstructed by Fogt (2009; SAMF), Abram et al. (2014; SAMA), and

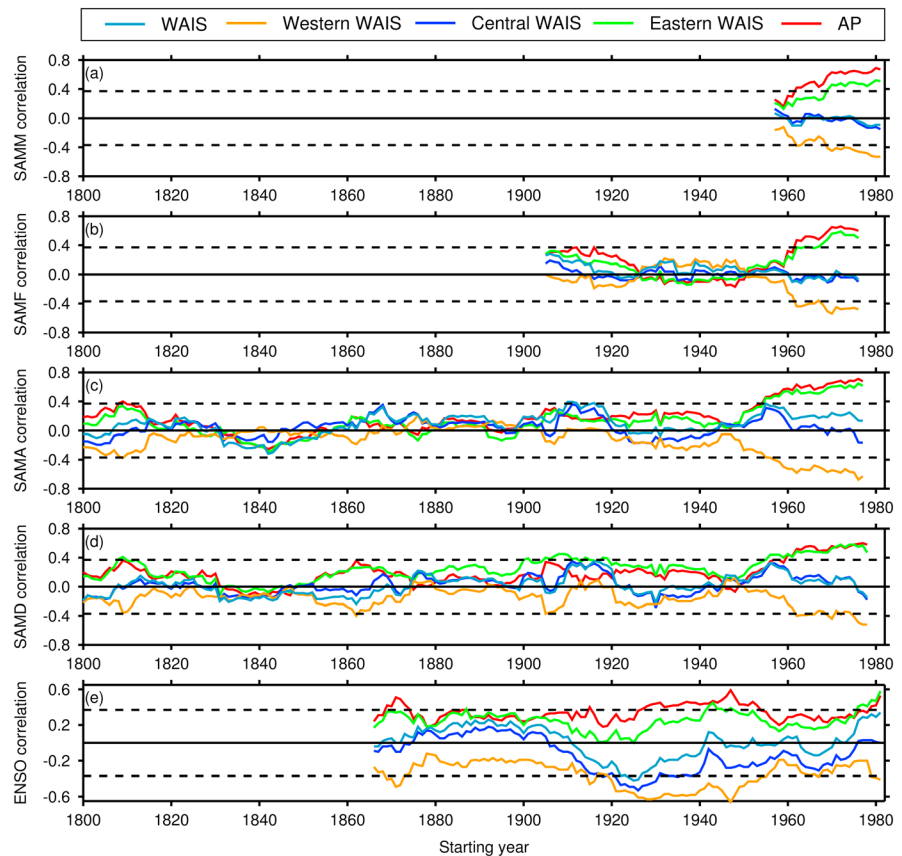


Figure 8. The 30-year running correlations between SMB reconstruction and SAM index by Marshall (2003; SAMM) for the 1957–2010 period (a), and the SAM indices reconstructed by Fogt (2009; SAMF) during 1905–2004 (b), Abram et al. (2014; SAMA) between 1800 and 2007 (c), and Dätwyler et al. (2018; SAMD) from 1800 to 2005 (d), and SOI index during 1866–2010 (e). The dashed lines denote the correlation coefficients with the significance at $p < 0.05$. WAIS = West Antarctic Ice Sheet; AP = Antarctic Peninsula.

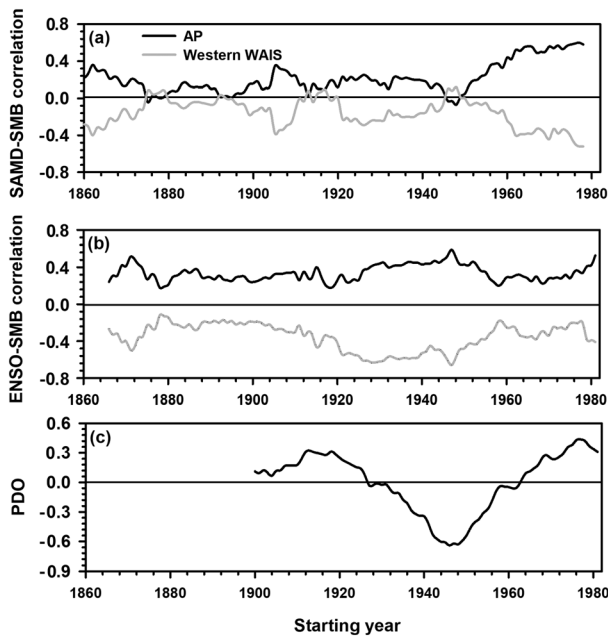


Figure 9. The 30-year running correlations between SMB reconstruction over the AP and western WAIS and (a) SAM index by Dätwyler et al. (2018) from 1860 to 2005, (b) Southern Oscillation Index during 1866–2010; (c) 30-yr running averaged PDO time series for the 1900–2010 period. SMB = surface mass balance; AP = Antarctic Peninsula; ENSO = El Niño–Southern Oscillation; WAIS = West Antarctic Ice Sheet; PDO = Pacific decadal oscillation.

Dätwyler et al. (2018; SAMD). The Southern Oscillation Index (SOI) is obtained from the Climatic Research Unit, University of East Anglia (Allan et al., 1991), which is a measure of the strength and phase of ENSO. The phase changes in the Pacific decadal oscillation (PDO) may influence the relationship between SAM and SMB (Goodwin et al., 2016). The PDO index is defined as the standardized principal component of monthly sea surface temperature anomalies over the North Pacific (poleward of 20°N). PDO index data come from Mantua (1997).

Annual SMB values averaged over the entire WAIS and central WAIS exhibit no significant correlation with the SAM reconstruction for the 1905–2004 and 1800–2005 periods (Table 1). Similarly, their correlations with observed SAM index during 1957–2010 are not statistically significant (Table 1). Running 30-year correlations reveal a generally weak relationship between SMB and SAM for these regions that reverses sign several times during the nineteenth and twentieth century (Figures 8b–8d). This suggests that the SAM has little impact on SMB averaged over the whole WAIS on decadal to centennial time scales. However, the SAM indices (SAMM, SAMD, SAMA, and SAMF) correlate generally positively with SMB over the AP and eastern WAIS ($r > 0.30$, $p < 0.01$), whereas significantly negative correlations are observed over the western WAIS ($r < -0.20$, $p < 0.01$) for their respective periods given in Table 1. To examine the temporal stability of these correlations, 30-year running correlations are calculated based on the time series of SMB and the SAM indices (Figures 8a–8d). It is apparent that all SAM indices show persistently robust correlations with the AP snow accumulation after ~1962, and western WAIS snow accumulation since ~1970. For the SAMA and SAMD time series, the 30-year running correlations are also significant

at the start of the record in ~1810. These suggest that the dipole in the spatial correlation pattern has occurred in the early nineteenth century but that the strength and duration of the positive (negative) SAM relationship in recent decades is unusual. The temporal instability of the regional relationship between SMB and the SAM may be associated with the phase of SAM, as reported by Goodwin et al. (2016). The deepening of the ASL is associated with a more positive SAM index (Raphael et al., 2016; Turner et al., 2013), which is confirmed by a period of significant SAM-ASL relationships since ~1960 (Figure S4) when a positive trend in the SAM was observed as reported by Abram et al. (2014). ASL deepening causes intensified northerly flow bringing warm moist air to the AP and the eastern WAIS and thus increasing snow accumulation in the region, but enhances the southerly flow over the western WAIS, drawing cold, dry air from continental Antarctica, which leads to the decrease in snow accumulation (Thomas et al., 2015; Wang et al., 2017; Figure S5). Thus, when the SAM becomes more positive, the relationship between the SAM and SMB over the AP, eastern and western WAIS becomes stronger. In the early nineteenth century, the SAM was briefly positive (Abram et al., 2014; Dätwyler et al., 2018). The SAM index has started to increase in the mid-1950s and shifted toward a greater frequency of the positive polarity from the post-1970s, more consistently positive during the past decade (e.g., Abram et al., 2014; Marshall, 2003), and thus, significant SAM-SMB correlations occur over that period.

For the entire period 1866–2010, no significant correlation is found between the SOI index and SMB over the whole WAIS and the central WAIS, but the correlations are significant over the AP, and eastern and western WAIS (Table 1). Running 30-year correlations (Figure 8e) suggest that significant SOI-SMB relationships over the AP and western WAIS occur for the records, which begin in ~1870, in the middle of the twentieth century and from 1980 onward. This may be associated with the strong dependence of ENSO's influence on West Antarctic climate on the strength and phase of the SAM (e.g., Clem & Fogt, 2013; Fogt et al., 2011; Wilson et al., 2014) and PDO (Goodwin et al., 2016; Gregory & Noone, 2008). Goodwin et al. (2016) reported the unstable correlations between snow accumulation time series from the Bruce Plateau ice core over the northwestern AP and the SAM and SOI during 1900–2009. The unstable relationships were as a function of the phase of both the SAM and PDO. We compare our reconstructed AP snow accumulation time

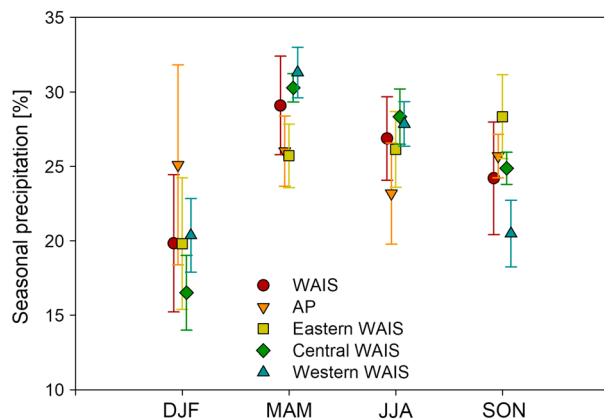


Figure 10. Contribution of seasonal precipitation to annual total over the AP, and eastern, central, and western WAIS, based on ERA-Interim data. WAIS = West Antarctic Ice Sheet; DJF = December-January-February; MAM = March-April-May; JJA = June-July-August; SON = September-October-November.

series and these ice core records. There is a weak and insignificant correlation ($r = 0.31$, $p = 0.06$) between the two time series from 1900 to 1939, whereas the correlation is strongly positive and statistically significant ($r = 0.81$, $p \ll 0.01$) for the 1940–2009 period (Figure S6). Because our reconstruction combines temporal variability in all available ice core records and spatial patterns of $P - E$ in ERA-Interim, our reconstructed time series are more representative for the AP snow accumulation variability than this ice core records. Given the robust agreement between the two time series since 1940s, the role of PDO in the temporally unstable correlations is analyzed (Figure 9). In the strengthening of the PDO beginning in the late-1940s and early-1950s in the 30-year running average, the running correlations between SAMD and SMB over the AP and western WAIS show a shift in sign, and the strongest SOI-SMB relationships occur. When the PDO is weakening, the running SAM-SMB correlations are weak, and the SOI-SMB correlations increase. In the middle of the twentieth century, when the SAM and PDO are under negative conditions, negative SOI (El Niño events) dominates, coinciding with low SMB over the AP and eastern WAIS, and high SMB over the western WAIS (Figure 6). Since ~1980, the

circulation conditions have shifted toward the positive phase of SAM (Marshall, 2003) and the negative polarity of PSA associated with ENSO variability (e.g., Ding et al., 2011; L'Heureux et al., 2013), which increases SMB over the AP and eastern WAIS and decreases SMB over the WAIS.

Abram et al. (2014) and Dätwyler et al. (2018) showed that, currently, the SAM is in its most persistent positive state for the past millennium. This long-term trend in the Antarctic circulation resembles conditions related to increased frequency and intensity of La Niña events (e.g., Ding et al., 2011; L'Heureux et al., 2013). The unprecedented trends in SMB over the AP and western WAIS can be explained by a similarly unprecedented positive phase of the SAM, coupled with a dominant La Niña phase, which amplifies the deepening of the ASL. In addition, we mention the possible roles of the stratospheric ozone depletion (Lenaerts et al., 2018) and recent atmospheric warming (Medley & Thomas, 2019).

ENSO events usually peak in the austral summer, especially in December (Turner, 2004). The recent trends in the SAM occur in the austral summer and autumn but are negligible in winter and spring (Marshall, 2003). SMB from ice core records is an annual total that is weighted by snowfall amounts during the year. The seasonality of WAIS precipitation and the two climate modes might constrain our comparison of SMB variability with SAM and SOI. However, their impacts on our comparison is very limited. Mean seasonal precipitation determined from ERA-Interim (1979–2012) shows weak seasonality over the AP (Figure 10), with a minimum of 23% of the annual precipitation in June-July-August and a maximum of 26% in March-April-May. Over the western WAIS and the whole WAIS, the largest precipitation is March-April-May, followed by June-July-August, and the smallest in December-January-February. Over the eastern WAIS, precipitation peaks in September-October-November, with the minimum in December-January-February. Despite these seasonal cycles, changes in the contribution of precipitation in each season to annual totals do not exceed 15% for each region (Figure 10). The statistically significant relationship between the seasonal SAMA and annual SMB time series over the AP and the western WAIS indicates that SAM in each season contributes to the annual SMB signal (Table S3). Both annual and seasonal SAM indices present no significant correlations with the SMB over the central WAIS and WAIS. For the 1866–2010 period, each seasonal SOI index, same as annual SOI index, significantly correlates with SMB time series over the AP, and eastern and western WAIS, but their relationship is insignificant on the central WAIS and the whole WAIS (Table S3).

4. Conclusions

A new SMB reconstruction over the WAIS is presented, to extend our knowledge of SMB variability across West Antarctica back to 1800. This new reconstruction fully accounts for the advantages of ice core records (time coverage), and strengths of both ERA-Interim and RACMO2.3p2 (spatial completeness), which better reproduces spatial patterns of WAIS SMB variability than a simple composite of the regional ice core snow accumulation records as performed by Thomas et al. (2017) and Wang et al. (2017). By comparing with our

reconstruction, spurious precipitation trends in ERA-Interim over the AP and eastern WAIS are identified. Thus, our reconstruction has the potential to examine the reliability of variability and trends in precipitation from other reanalysis products and climate models. It is also useful for studying the WAIS mass balance variability.

When averaged over the whole WAIS, SMB shows a significantly negative trend (-1.9 ± 2.2 Gt/year per decade, $p < 0.01$) during the nineteenth century, but a significantly positive trend (5.4 ± 2.9 Gt per decade, $p < 0.01$) in the twentieth century. This is not consistent with the previously reported insignificant changes in snow accumulation over the WAIS during the past 50 years (Monaghan et al., 2006) and 200 years (Frezzotti et al., 2013). One possible explanation is the lack of recent ice core records in the AP and coastal zones in these studies and a high weight given to cores from the interior of Antarctica. At regional scales, we find a strong dipole pattern in SMB during the first half of the nineteenth century and the second half of the twentieth century, with the positive trends at the AP and on the eastern WAIS, and the contrasting negative trends on the western WAIS during the past 50 years. These recent trends are unprecedented for the last 200 years. We suggest a limited influence of SAM and ENSO on the variability in SMB over the entire WAIS during the past 200 years. SMB over the AP and western WAIS show significant correlations with SAM and ENSO. However, the significant correlations are not stable in time, which is related to changes in the phase of SAM, SOI and PDO. The unprecedented trends during the past 50 years are related to the positive polarity of the SAM and dominant La Niña events that have resulted in a deepening of the ASL, leading to warm, moist northerly flow to the AP and eastern WAIS, and cold, dry southerly flow to the western WAIS.

Acknowledgments

This work was funded by the Strategic Priority Research Program of the Chinese Academy of Sciences (XAD19070103), the Outstanding Youth Fund of Shandong Provincial Universities (ZR2016JL030), and the National Natural Science Foundation of China (41576182). M. R. van den Broeke and J. M. van Wessem acknowledge support from the Netherlands Polar Program and the Netherlands Earth System Science Center (NESSC). Snow accumulation data is a contribution to the PAGES 2k Network through the Antarctica 2k and CLIVASH2k projects. Past Global Changes (PAGES) is funded by the U.S. National Science Foundation and the Swiss Academy of Sciences. Thanks to the three anonymous reviewers for their constructive and thoughtful comments and advice to improve this paper. ERA-Interim data are obtained from ECMWF data server (<http://apps.ecmwf.int/datasets/>). HadSLP2 data are provided by Met Office Hadley Centre observations datasets (<http://www.metoffice.gov.uk/hadobs/hadslp2/>). SAM index developed by Abram et al. (2014) comes from ftp://ftp.ncdc.noaa.gov/pub/data/paleo/contributions_by_author/abram2014/abram2014sam.txt. SOI developed by Allan et al. (1991) is available at <http://www.cru.uea.ac.uk/cru/data/soi/>. Ice core snow accumulation data are available at <https://doi.org/10.5285/c4ecfe25-12f2-453b-ad19-49a19e90ee32>. PDO data are hosted at <http://research.jisao.washington.edu/data/pdo/> website. RACMO2.3p2 accumulation fields can be obtained from M. R. van de Broeke and J. M. van Wessem without conditions. Snow accumulation data reconstructed by Medley and Thomas (2019) come from the NASA Goddard Cryosphere data portal (<https://neptune.gsfc.nasa.gov/csb/>). Our reconstructed WAIS SMB data are available at <http://poles.tpcd.ac.cn/> website.

References

- Abram, N. J., Mulvaney, R., Vimeux, F., Phipps, S. J., Turner, J., & England, M. H. (2014). Evolution of the southern annular mode during the past millennium. *Nature Climate Change*, *4*(7), 564–569. <https://doi.org/10.1038/nclimate2235>
- Agosta, C., Favier, V., Krinner, G., Gallée, H., Fettweis, X., & Genthon, C. (2013). High-resolution modelling of the Antarctic surface mass balance, application for the twentieth, twenty first and twenty second centuries. *Climate Dynamics*, *41*(11–12), 3247–3260. <https://doi.org/10.1007/s00382-013-1903-9>
- Allan, R. J., Nicholls, N., Jones, P. D., & Butterworth, I. J. (1991). A further extension of the Tahiti-Darwin SOI, early ENSO events and Darwin pressure. *Journal of Climate*, *4*(7), 743–749. [https://doi.org/10.1175/15200442\(1991\)004<0743:AFEOTT>2.0.CO;2](https://doi.org/10.1175/15200442(1991)004<0743:AFEOTT>2.0.CO;2)
- Bamber, J. L., Riva, R., Vermeersen, B., & LeBrocq, A. (2009). Reassessment of the potential sea-level rise from a collapse of the West Antarctic Ice Sheet. *Science*, *324*(5929), 901–903. <https://doi.org/10.1126/science.1169335>
- Bromwich, D. H., Nicolas, J. P., & Monaghan, A. J. (2011). An assessment of precipitation changes over Antarctica and the Southern Ocean since 1989 in contemporary global reanalyses. *Journal of Climate*, *24*(16), 4189–4209. <https://doi.org/10.1175/2011JCLI4074.1>
- Clem, K. R., & Fogt, R. L. (2013). Varying roles of ENSO and SAM on the Antarctic Peninsula climate in austral spring. *Journal of Geophysical Research: Atmospheres*, *118*, 11,481–11,492. <https://doi.org/10.1002/jgrd.50860>
- Dätwyler, C., Neukom, R., Abram, N. J., Gallant, A. J. E., Grosjean, M., Jacques-Coper, M., et al. (2018). Teleconnection stationarity, variability and trends of the Southern Annular Mode (SAM) during the last millennium. *Climate Dynamics*, *51*(5–6), 2321–2339. <https://doi.org/10.1007/s00382-017-4015-0>
- Dee, D. P., Uppala, S. M., Simmons, A. J., Berrisford, P., Poli, P., Kobayashi, S., et al. (2011). The ERA-Interim reanalysis: Configuration and performance of the data assimilation system. *Quarterly Journal of the Royal Meteorological Society*, *137*(656), 553–597. <https://doi.org/10.1002/qj.828>
- Ding, Q., Steig, E. J., Battisti, B. S., & Küttel, M. (2011). Winter warming in West Antarctica caused by central tropical Pacific warming. *Nature Geoscience*, *4*(6), 398–403. <https://doi.org/10.1038/ngeo1129>
- Fogt, R. L. (2009). Seasonal Southern Hemisphere annular mode (SAM) reconstructions. Byrd Polar and Climate Research Center. Retrieved from http://polarmet.osu.edu/ACD/sam/sam_recon.html
- Fogt, R. L., Bromwich, D. H., & Hines, K. M. (2011). Understanding the SAM influence on the South Pacific ENSO teleconnection. *Climate Dynamics*, *37*(9–10), 2127–2128. <https://doi.org/10.1007/s00382-011-1201-3>
- Fogt, R. L., Clark, L. N., & Nicolas, J. P. (2018). A new monthly pressure dataset poleward of 60°S since 1957. *Journal of Climate*, *31*(10), 3865–3874. <https://doi.org/10.1175/JCLI-D-17-0879>
- Frezzotti, M., Scarchilli, C., Becagli, S., Proposito, M., & Urbini, S. (2013). A synthesis of the Antarctic surface mass balance during the last 800 yr. *The Cryosphere*, *7*(1), 303–319. <http://doi.org/10.5194/tc-7-303-2013>
- Frieler, K., Clark, P. U., He, F., Buizert, C., Reese, R., Ligtenberg, S. R. M., et al. (2015). Consistent evidence of increasing Antarctic accumulation with warming. *Nature Climate Change*, *5*(4), 348–352. <https://doi.org/10.1038/nclimate2574>
- Fudge, T. J., Markle, B. R., Cuffey, K. M., Buizert, C., Taylor, K. C., Steig, E. J., et al. (2016). Variable relationship between accumulation and temperature in West Antarctica for the past 31,000 years. *Geophysical Research Letters*, *43*, 3795–3803. <https://doi.org/10.1002/2016GL068356>
- Genthon, C., & Cosme, E. (2003). Intermittent signature of ENSO in west-Antarctic precipitation. *Geophysical Research Letters*, *30*(21), 2081. <https://doi.org/10.1029/2003GL018280>
- Goodwin, B. P., Mosely-Thompson, E., Wilson, A. B., Porter, S. E., & Sierra Hernandez, M. R. (2016). Accumulation variability in the Antarctic Peninsula: The role of large-scale atmospheric oscillations and their interactions. *Journal of Climate*, *122*(7–8), 1135–1159. <https://doi.org/10.1130/B30079.1>
- Gregory, S., & Noone, D. (2008). Variability in the teleconnection between the El Niño Southern Oscillation and West Antarctic climate deduced from West Antarctic ice core isotope records. *Journal of Geophysical Research*, *113*, D17110. <https://doi.org/10.1029/2007JD009107>

- Kaspari, S., Mayewski, P. D., Dixon, D. A., Spikes, V. B., Sneed, S., Handley, M. J., & Hamilton, G. S. (2004). Climate variability in West Antarctica derived from annual accumulation-rate records from ITASE firn/ice cores. *Annals of Glaciology*, *39*, 585–594. <https://doi.org/10.3189/172756404781814447>
- L'Heureux, M. L., Lee, S., & Lyon, B. (2013). Recent multidecadal strengthening of the Walker circulation across the tropical Pacific. *Nature Climate Change*, *3*(6), 571–576. <https://doi.org/10.1038/NCLIMATE1840>
- Lenaerts, J. T. M., Fyke, J., & Medley, B. (2018). The signature of ozone depletion in recent Antarctic precipitation change: A study with the Community Earth System Model. *Geophysical Research Letters*, *45*, 12,931–12,939. <https://doi.org/10.1029/2018GL078608>
- Lenaerts, J. T. M., van den Broeke, M. R., van de Berg, W. J., van Meijgaard, E., & Kuipers Munneke, P. (2012). A new, high-resolution surface mass balance map of Antarctica (1979–2010) based on regional atmospheric climate modeling. *Geophysical Research Letters*, *39*, L04501. <https://doi.org/10.1029/2011GL050713>
- Mantua, N. J. (1997). PDO Index. University of Washington. Retrieved from <http://jisao.washington.edu/pdo/PDO.latest>
- Marshall, G. J. (2003). An observation-based Southern Hemisphere annular mode index. British Antarctic Survey. Retrieved from <http://www.nerc-bas.ac.uk/icd/gjma/sam.html>
- Marshall, G. J., Thompson, D. W. J., & van den Broeke, M. R. (2017). The signature of Southern Hemisphere atmospheric circulation patterns in Antarctic precipitation. *Geophysical Research Letters*, *44*, 11,580–11,589. <https://doi.org/10.1002/2017GL075998>
- Medley, B., Joughin, I., Das, S. B., Steig, E. J., Conway, H., Gogineni, S., et al. (2013). Airborne-radar and ice-core observations of annual snow accumulation over Thwaites Glacier, West Antarctica confirm the spatiotemporal variability of global and regional atmospheric models. *Geophysical Research Letters*, *40*, 3649–3654. <https://doi.org/10.1002/grl.50706>
- Medley, B., & Thomas, E. R. (2019). Increased snowfall over the Antarctic Ice Sheet mitigated twentieth-century sea-level rise. *Nature Climate Change*, *9*(1), 34–39. <https://doi.org/10.1038/s41558-018-0356-x>
- Mo, K. C., & Higgins, R. W. (1998). The Pacific-South American modes and tropical convection during the Southern Hemisphere winter. *Monthly Weather Review*, *126*(6), 1581–1596. [https://doi.org/10.1175/1520-0493\(1998\)126%3C1581:TPSAMA%3E2.0.CO;2](https://doi.org/10.1175/1520-0493(1998)126%3C1581:TPSAMA%3E2.0.CO;2)
- Monaghan, A. J., Bromwich, D. H., Fogt, R. L., Wang, S.-H., Mayewski, P. A., Dixon, D. A., et al. (2006). Insignificant change in Antarctic snowfall since the international geophysical year. *Science*, *313*(5788), 827–831. <https://doi.org/10.1126/science.1128243>
- Mouginot, J., Rignot, E., & Scheuchl, B. (2014). Sustained increase in ice discharge from the Amundsen Sea Embayment, West Antarctica, from 1973 to 2013. *Geophysical Research Letters*, *41*, 1576–1584. <https://doi.org/10.1002/2013GL059069>
- Nicolas, J. P., & Bromwich, D. H. (2014). New reconstruction of Antarctic near-surface temperatures: Multidecadal trends and reliability of global reanalyses. *Journal of Climate*, *27*(21), 8070–8093. <https://doi.org/10.1175/JCLI-D-13-00733.1>
- Raphael, M. N., Marshall, G. J., Turner, J., Fogt, R. L., & Schneider, D. (2016). The Amundsen Sea Low: Variability, Change, and Impact on Antarctic Climate. *Bulletin of the American Meteorological Society*, *97*(1), 111–121. <https://doi.org/10.1175/BAMS-D-14-00018.1>
- Rignot, E. (2008). Changes in West Antarctic ice stream dynamics observed with ALOS PALSAR data. *Geophysical Research Letters*, *35*, L12505. <https://doi.org/10.1029/2008GL033365>
- Rotschky, G., Holmlund, P., Isaksson, E., Mulvaney, R., Oerter, H., Van den Broeke, M. R., & Winther, J. G. (2007). A new surface accumulation map for western Dronning Maud Land, Antarctica, from interpolation of point measurements. *Journal of Glaciology*, *53*(182), 385–398. <https://doi.org/10.3189/002214307783258459>
- Schneider, D. P., Okumura, Y., & Deser, C. (2012). Observed Antarctic interannual climate variability and tropical linkages. *Journal of Climate*, *25*(12), 4048–4066. <https://doi.org/10.1175/JCLI-D-11-00273.1>
- Shepherd, A., Ivins, E., Rignot, E., Smith, B., van den Broeke, M., Velicogna, I., et al. (2018). Mass balance of the Antarctic Ice Sheet from 1992 to 2017. *Nature*, *558*(7709), 219–222. <https://doi.org/10.1038/s41586-018-0179-y>
- Thomas, E. R., Hosking, J. S., Tuckwell, R. R., & Ludlow, E. C. (2015). Twentieth century increase in snowfall in coastal West Antarctica. *Geophysical Research Letters*, *42*, 9387–9393. <https://doi.org/10.1002/2015GL065750>
- Thomas, E. R., Marshall, G. J., & McConnell, J. R. (2008). A doubling in accumulation in the western Antarctic Peninsula since 1850. *Geophysical Research Letters*, *35*, L01706. <https://doi.org/10.1029/2007GL032529>
- Thomas, E. R., van Wessem, J. M., Roberts, J., Isaksson, E., Schlosser, E., Fudge, T. J., et al. (2017). Regional Antarctic snow accumulation over the past 1000 years. *Climate of the Past*, *13*(11), 1491–1513. <https://doi.org/10.5194/cp-13-1491-2017>
- Turner, J. (2004). The El Niño-Southern Oscillation and Antarctica. *International Journal of Climatology*, *24*, 1–31. <https://doi.org/10.1002/joc.965>
- Turner, J., Phillips, T., Hosking, J. S., Marshall, G. J., & Orr, A. (2013). The Amundsen Sea low. *International Journal of Climatology*, *33*(7), 1818–1829. <https://doi.org/10.1002/joc.3558>
- Van de Berg, W. J., & Medley, B. (2016). Brief Communication: Upper-air relaxation in RACMO₂ significantly improves modelled inter-annual surface mass balance variability in Antarctica. *The Cryosphere*, *10*, 459–463. <https://doi.org/10.5194/tc-10-459-2016>
- Van de Berg, W. J., Van den Broeke, M. R., Reijmer, C., & Van Meijgaard, E. (2006). Reassessment of the Antarctic surface mass balance using calibrated output of a regional atmospheric climate model. *Journal of Geophysical Research*, *111*, D11104. <https://doi.org/10.1029/2005JD006495>
- Van Wessem, J. M., Reijmer, C. H., Morlighem, M., Mouginot, J., Rignot, E., Medley, B., et al. (2014). Improved representation of East Antarctic surface mass balance in a regional atmospheric climate model. *Journal of Glaciology*, *60*(222), 761–770. <https://doi.org/10.3189/2014JG14J051>
- Van Wessem, J. M., van de Berg, W. J., Noël, B. P. Y., van Meijgaard, E., Amory, C., Birnbaum, G., et al. (2018). Modelling the climate and surface mass balance of polar ice sheets using RACMO2—Part 2: Antarctica (1979–2016). *The Cryosphere*, *12*(4), 1479–1498. <https://doi.org/10.5194/tc-12-1479-2018>
- Wang, Y., Ding, M., van Wessem, J., Schlosser, E., Altnau, S., van den Broeke, M., et al. (2016). A comparison of Antarctic Ice Sheet surface mass balance from atmospheric climate models and in situ observations. *Journal of Climate*, *29*(14), 5317–5337. <https://doi.org/10.1175/JCLI-D-15-0642.1>
- Wang, Y., Hou, S., Sun, W., Lenaerts, J. T. M., van den Broeke, M. R., & van Wessem, J. M. (2015). Recent surface mass balance from Syowa Station to Dome F, East Antarctica: Comparison of field observations, atmospheric reanalyses, and a regional atmospheric climate model. *Climate Dynamics*, *45*(9–10), 2885–2899. <https://doi.org/10.1007/s00382-015-2512-6>
- Wang, Y., Thomas, E. R., Hou, S., Huai, B., Wu, S., Sun, W., et al. (2017). Snow accumulation variability over the West Antarctic Ice Sheet since 1900: A comparison of ice core records with ERA-20C reanalysis. *Geophysical Research Letters*, *44*, 11,482–11,490. <https://doi.org/10.1002/2017GL075135>
- Wilson, A. B., Bromwich, D. H., Hines, K. M., & Wang, S. (2014). El Niño flavors and their simulated impacts on atmospheric circulation in the high southern latitudes. *Journal of Climate*, *27*(23), 8934–8955. <https://doi.org/10.1175/JCLI-D-14-00296.1>
- Wouters, B., Martín-Español, A., Helm, V., Flament, T., van Wessem, J. M., Ligtenberg, S. R. M., et al. (2015). Dynamic thinning of glaciers on the Southern Antarctic Peninsula. *Science*, *348*(6237), 899–903. <https://doi.org/10.1126/science.aaa5727>